sciendo
DOI: 10.2478/eces-2024-0027 ECOL CHEM ENG S. 2024;31(3):397-409

Xinjian FAN[1*], Jiahui ZHANG[1], Wei YAO[1], Chunhai DONG[1], Lirong WANG[1] and Hao TIAN[1]

INFLUENCE OF DIFFUSION ANGLE ON SEDIMENT CONCENTRATION IN FRONT INFLOW FOREBAY OF PUMPING STATION

Abstract: The numerical simulation and field investigation of solid-liquid two-phase flow are carried out in a large-scale forward intake forebay with various diffusion angles at the Jingtaichuan Pumping Irrigation Project in Gansu Province, China. The purpose is to investigate the properties of sediment deposition in the pumping station forebay. The results indicate that the low-sediment concentration area is in the forebay's centre, whereas the high-sediment is near the two side walls flanks. The sediment concentration increases dramatically from the centre to the sides. Both the high-sediment concentration area and the sediment concentration increase with water depth. The forebay's narrowing diffusion angle causes the high-concentration area to gradually decrease while the low-concentration area gradually increase. Furthermore, the amount of siltation and sediment deposition efficiency decrease, resulting in a large increase in forebay sediment concentration and sedimentation efficiency. The sediment concentration and water flow velocity reveal a quadratic polynomial relationship. This study can provide a guide and reference for the design and construction of comparable large-scale pumping station forebays.

Keywords: front inflow forebay, diffusion angle, numerical modelling, sediment concentration, sediment efficiency

Introduction

In current society, the advancement of green innovation plays a vital role in fostering sustainable development. To achieve this goal, Zhao et al. [1] utilised panel data from carbon emission trading pilot projects and applied the Spatial Durbin Model (SDID) to evaluate the effects of carbon trading on corporate environmental responsibility. Additionally, Li et al. [2] employ factor analysis and fuzzy comprehensive evaluation methods to thoroughly assess the foundational advantages, growth prospects, and sustainability of various industries. Moreover, understanding the sedimentation characteristics in the forebay of pump stations is a critical issue in ongoing research, aimed at enhancing green development initiatives. The hydraulic performance of forebays in engineering have a huge impact on flow patterns [3-5]. Hyperconcentrated flow at pumping stations can lead to vortexes and sediment buildup in forebays, reducing water flow capacity and pump efficiency. This can negatively impact irrigation capacity, crop yield,

[1] School of Energy and Power Engineering, Lanzhou University of Technology, Lanzhou 730050, China, email: Fanxj008@163.com, 1909594314@qq.com, 945172552@qq.com, 953454575@qq.com, 3386904976@qq.com, 1274608794@qq.com, ORCID: XF 0000-0002-9261-053X, JZ 0009-0001-2968-5459, WY 0009-0001-6589-7950, CD 0009-0008-2500-5082, LW 0009-0009-6599-3748, HT 0009-0003-6046-6734
[*] Corresponding author: Fanxj008@163.com

and overall economic benefits of the project [6-8]. The serious silting problems in pump station forebays were address by many researchers. Some good diversion measurements, such as flow deflectors [9, 10], bottom sills [11], baffles [12-14], and partition piers [15], were applied in engineering. The simulation optimization of the size and the structure of the forebays were also proposed [16, 17]. Some new combined rectification facilities [18, 19] and other methods [20-22] were tried in projects as well. These measures optimise reservoir flow patterns, minimise high-velocity water impacts, boost sediment transport capacity, and reduce sediment deposition. However, the proposed anti-silting and rectification measures are mostly localised improvements. Research on the influence of forebay size and structure optimization, especially the large-scale profile of forebays and the impact on the distribution of sediments have been unclear.

This study focuses on the characteristics of a forebay in Jingtaichuan Pumping Irrigation Project of Gansu Province, China. Based on field investigation and numerical calculation methods, the study explores the distribution of sediment concentration influenced by the expansion angle of the flank wall in the front inflow forebay. It aims at the distribution characteristics and sedimentation mechanism of the front inflow forebay. This study provides a guide and reference for the design and construction of similar large-scale pumping stations.

Fundamental state

Project profile

The Jingtaichuan Pumping irrigation project is China's first multi-stage power irrigation project with high head and flow. It contains a total of 43 pumping stations. This project has brought about a thorough change to local agricultural production, delivering significant engineering and social benefits to the hydroelectric irrigation district.

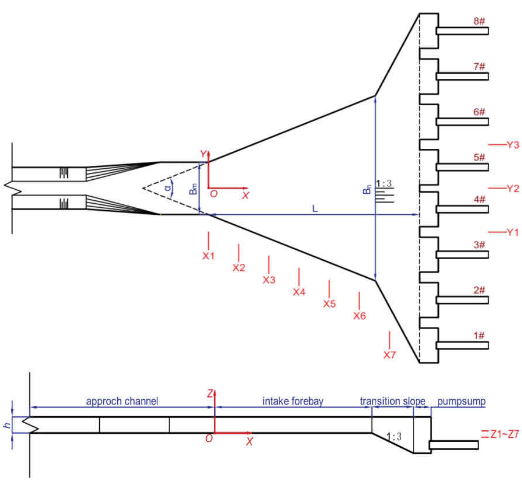

Fig. 1. Schematic of the front inflow pumping station forebay

Figure 1 depicts a schematic of a front inflow forebay from a pump station in the project. The design water flow rate is 23 m^3/s, and the front pool's design water level is

1591.83 meters. The front pool has a diffusion angle of α = 46° between the flank wall of the inflow forebay and the incoming water flow. After a length of L = 33.83 m and a gradual slope of 1/3 at the bottom of the pool, 8 pumping units are placed in the ultimate breadth of B_n = 40.42 m. In general, six pump units work properly, with the exception of pump units 1# and 8#, which are used for standby. The pool has a depth of h = 3.97 m, and a total surface area of S_0 = 1400.10 m^2.

Field investigation

The pump station's water inflow has an annual average silt mass concentration of around 30 kg/m^3. During the flood season, the maximum silt mass concentration may reach to 326 kg/m^3. The particle size distribution of suspended sediment in the pool ranges from 0.02 mm to 1 mm, with more that 90 % of particles less than 0.063 mm [23]. The high concentration of tiny sediment-laden stream might quickly result in significant sediment accumulation in the front pool.

a) b)

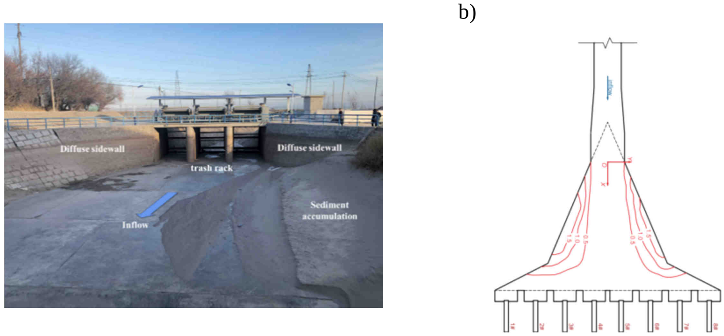

Fig. 2. a) A sediment deposition during field investigation, b) the corresponding contour map of sediment deposition in the front inflow pumping station forebay

A large amount of silt deposition was discovered in the pump station pool during field investigation, as illustrated in Figure 2a. The silt is most concentrated at the sidewalls, and it is distributed symmetrically along the pool's centre line. Sediment accumulation steadily declines from the sidewalls to the centre flow, as illustrated by the contour map of sediment deposition in Figure 2b. The sediment's highest thickness was measured at 1.5 m. The entire siltation area was approximately 470 m^2, almost one-third of the pool. As a result, it inhibits water flow capacity and considerably reduces the regulated volume of the front pool. The efficiency of the pump station would thereafter be dramatically reduced.

Mathematical model

Governing equations

The forebay flow is a solid-liquid two-phase flow that can be termed incompressible. The mixture model is used to represent the solid-liquid two-phase flow because it accurately simulates the features of water and sediment movement [24]. The mixing model's continuity equation and the motion equation are shown below:

$$\frac{\partial}{\partial t}(\rho_m) + \nabla\cdot(\rho_m \vec{v}_m) = 0 \tag{1}$$

$$\frac{\partial}{\partial t}(\rho_m v_m) + \nabla\cdot(\vec{v}_m \vec{v}_m) = -\nabla_p + \nabla\cdot[\mu_m(\nabla\vec{v}_m + \nabla\vec{v}_m^T)]\vec{F} + \nabla\cdot\left(\sum_{k=1}^{n} \alpha_k \rho_k \vec{v}_{dr,k} \vec{v}_{dr,k}\right) \tag{2}$$

In which, $\rho_m = \sum_{k=1}^{n} \alpha_k \rho_k$, $\vec{v}_m = \frac{\sum_{k=1}^{n} \alpha_k \rho_k \vec{v}_k}{\rho_m}$, $\mu_m = \sum_{k=1}^{n} \alpha_k \mu_k$, $\vec{v}_{dr,k} = \vec{v}_k - \vec{v}_m$.

where, ρ_m is mixed fluid density, ρ_k is the density of the kth phase, α_k is the volume fraction of the *k* phase, $\vec{v}_m$ is the average velocity of mass, *p* is the flow field pressure, *n* is the phase number, μ_m is the mixed fluid viscosity coefficient, μ_k is the *k*-phase turbulent viscosity coefficient, $\vec{g}$ is gravity acceleration, $\vec{F}$ is volume force, and $\vec{v}_{dr,k}$ is the velocity of sub-equal *k* phase.

Turbulence model

The *k*-*ε* turbulence model is commonly used to simulate complex turbulent three-dimensional motion in engineering. The realizable *k*-*ε* turbulence model is used for numerical modelling of water and sediment flow in the front pool. The *k*-equation and *ε*-equation are shown in equations (3) and (4) [25]:

$$\frac{\partial(\rho k)}{\partial t} + \frac{\partial(\rho k u_i)}{\partial x_i} = \frac{\partial}{\partial x_j}\left[\left(\mu + \frac{\mu_t}{\sigma_k}\right)\frac{\partial k}{\partial x_j}\right] + G_k - \rho\varepsilon \tag{3}$$

$$\frac{\partial(\rho\varepsilon)}{\partial t} + \frac{\partial(\rho\varepsilon u_i)}{\partial x_i} = \frac{\partial}{\partial x_j}\left[\left(\mu + \frac{\mu_t}{\sigma_\varepsilon}\right)\frac{\partial\varepsilon}{\partial x_j}\right] + \rho C_1 E\varepsilon - \rho C_2 \frac{\varepsilon^2}{k + \sqrt{v\varepsilon}} \tag{4}$$

in which: $C_1 = \max\left(0.43, \frac{\eta}{\eta+5}\right)$, $\eta = \frac{k}{\varepsilon}\cdot(2E_{ij}E_{ij})^{1/2}$, $E_{ij} = \frac{1}{2}\left(\frac{\partial u_i}{\partial x_j} + \frac{\partial u_j}{\partial x_I}\right)$, $\mu_t = \rho C_\mu \frac{k^2}{\varepsilon}$, $C_\mu = \frac{1}{A_0 + A_S U^* k/\varepsilon}$, where: $\sigma_k = 1.0$, $\sigma_\varepsilon = 1.2$, and $C_2 = 1.9$.

Boundary conditions

The forebay's intake is configured as a velocity inlet, with a velocity of 1.71 m/s. The forebay's exit is designated as a free outflow [26]. The free surface is assumed to be stiff and set to symmetry. The remaining walls are treated using wall functions [27].

The two-phase flow comprises of water and sand. Water is the main phase and has a density of ρ_w = 998.2 kg/m^3. Sand is the secondary phase, with a density of ρ_s = 2500 kg/m^3. The sand particle size is set to *d* = 0.025 mm. The volume of sediment concentration is fixed at C_0 = 1.2 % for the inlet conduit. The convection is calculated using a second-order upwind approach. The SIMPLEC technique is used for numerical simulation, with iteration residual precision greater than 10^{-4} [28].

Figure 3 shows the mesh divisions. The ICEM software is used to create unstructured meshes for 3*D* geometric models. After conducting grid independence tests, the optimal grid size is determined to be 0.35 m. A total of 2.505 million mesh cells are used, and the mesh quality is more than 0.3.

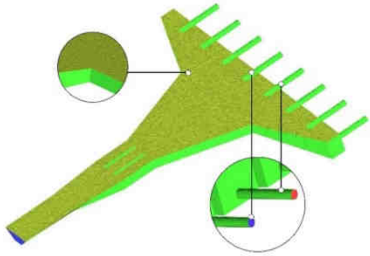

Fig. 3. The meshes of the pumping station forebay

Simulation conditions

The diffusion angle of the side wall, α, has a significant impact on the sediment concentration distribution in forebays. This study models six forebays with varying diffusion angles of α = 20°, 25°, 30°, 35°, 40°, and 46°. The prototype for Jingtaichuan pumping station has a final angle of α = 46°.

The simulation condition represents the regular operating situation, with units No. 2#-7# working and the units No. 1# and 8# on standby. The origin of coordinates, O, lies at the base of the water arriving centre line, at which the sidewalls of the forebay begin to grow. The three dimension axis directions are the *X*-direction of the incoming water flow direction, the *Y*-direction of the horizontal direction perpendicular to the *X*-direction, and the upward *Z*-direction (shown as in Fig. 1). There are six points on the *X*-axis, which is from 0 m to 30 m every six meters. Three points are located in *Y*-axis, which is –9.58 m, 0 m and 9.58 m. From the bottom upward, seven sections of *Z*-direction are selected from 0.2 meter to 1.4 meters every point two meters.

To clearly examine sediment distribution, intersection lines in each plane are used for better observations. For example, the line in the *XOZ* plane is labelled as $l_{X1\text{-}Z1}$. The dimensionless sediment concentration in the forebay is $C^* = C/C_0$, C is the sediment concentration, and C_0 is the average inlet flow sediment concentration. The dimensionless surface area of the forebay is $S^* = S/S_0$, S is the highest sediment concentration area, and S_0 is the surface area of the forebay. The observation parameters are illustrated in Table 1.

Table 1

Observation parameters for simulation section

Name	Dimensionless symbol	Calculation equation	Value	Notes
Along the vertical inflow Direction *X* [m]	X^*	$X^* = X/B_m$	X = (0-30) m (every 6 m) B_m = 11.7 m	B_m is the front width
Along the water depth *Z* [m]	Z^*	$Z^* = Z/h$	Z = (0.2-1.4) m (every 0.2 m) h = 3.97 m	*h* is the pool has a depth
Sediment concentration *C* [%]	C^*	$C^* = C/C_0$	C_0 = 1.2 % C^*= 0.751-1.252	C_0 is the average inlet flow sediment concentration
Area of high sediment [m²] Concentration region, *S*	S^*	$S^* = S/S_0$	S_0 = 1400.10 m² S^* = 0.017-0.12	S_0 is the surface area of the forebay

Results

Flow field

Figure 4 depicts the flow field in the front flow forebay. The large diffusion angle of the sidewall weakens the flow constraint ability and creates a certain angle between the incoming flow and the sidewall, resulting in significant flow detachment from the wall. The flow field has a symmetrical distribution. The central section depicts the main flow region, with high velocity and a stable flow state. The sides are backflow regions, with slow velocities and turbulent flow. In reflux regions, there are two large-scale elliptical vortexes, with intensities and velocities increasing from center to edge. The vortices limit the main flow's expansion. As a result, the flow velocity reduces and the sediment-carrying capacity weakens, leading to sediment deposition and diminishing the pump efficiency.

When the diffusion angle of the front pool decreases (as seen in Fig. 4a-c), the sidewalls hinder the flow less, and flow detachment from the walls weakens. The compressive effect of vortexes in backflow regions eventually decreases. The percentage of the primary flow region grows, as does the diffusion efficiency. Figure 4c when the diffusion angle is reduced to 20°, the vortexes in backflow regions nearly disappear. However, the vortex transfers continue to depart, and some low-velocity patches form, worsening the flow in the forebay. Conclusively, lowering the diffusion angle of the front inlet forebay can improve flow patterns and stability. However, an excessively tiny diffusion angle would be rejected because it would limit the expansion of main flow, increasing the flow velocity. The high velocity would then immediately contact the pump blades, resulting in extremely poor operating conditions at the pump station.

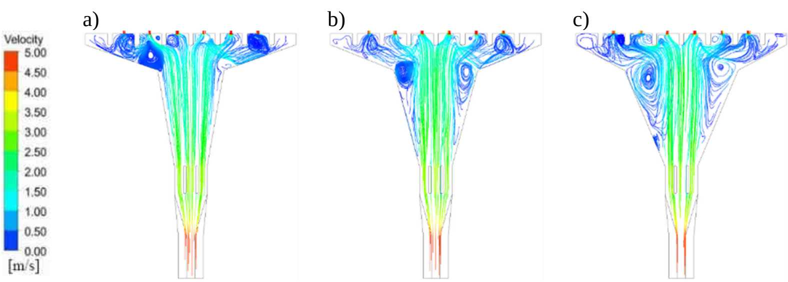

Fig. 4. The diagrams of flow patterns in the inlet forebay of forward inflow pump station with a) $\alpha = 46°$, b) $\alpha = 30°$, c) $\alpha = 20°$

Effect of the angle *α* on sediment deposition

Figure 5 depicts the variation in sediment concentration in the horizontal *Z*2 segment with different diffusion angles of the forebay. The sediment content is assumed to be high when it surpasses 1.32 %; otherwise, it is low. Thus, the sediment concentration in the centre of the forepond is low, whereas it is high near the two sidewalls.

In the prototype pump station with a front pool diffusion angle of $\alpha = 46°$, sediment accumulation in the backflow regions is severe, as shown in Figure 5a. Its high concentration region occupies almost 71 % of the surface area of the forebay. When the diffusion angle decreases, the high concentration area shrinks. For instance, when the angle $\alpha = 40°$, the forebay has a high concentration of around 61.11 %. When the angle $\alpha = 20°$, the high concentration is only about 24.52 % of the forebay, reducing by nearly 46.48 % compared to the prototype forebay. Conversely, as the diffusion angle decreases, the low concentration area increase. Figures 5b and c indicate a 24.14 % increase at the minimal angle. Figure 5 shows that the high concentration area changes from an elliptical to an elongated strip as the angle *α* decreases. It is primarily owing to the lesser vortexes in the backflow regions. At this point, flow velocity of the main stream remains high, and its sediment-carrying capacity increases. As a result, sediment mitigate occurs at the forebay's narrow diffusion angle.

Actually, even the small diffusion angle can reduce sediment concentration and buildup, whereas a narrow diffusion section can limit flow expansion. It would produce a direct high impact flow with high velocity shocks on the pump units, causing equipment damage and lowering efficiency. Meanwhile, both sides of the diffusion section have been relatively unaffected, resulting in low-velocity or stagnant water zones. This may lead to secondary sediment accumulation.

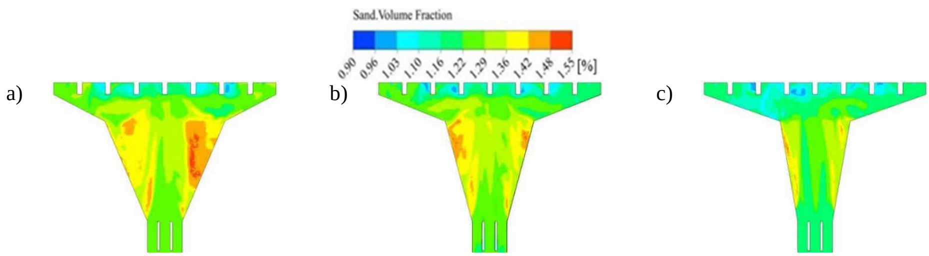

Fig. 5. Sediment concentration distribution in the horizontal *Z*1 section of the forebay with a) α = 46°, b) α = 30°, c) α = 20°

Sediment along the flow with different depths

The fluctuation in sediment concentration along the water flow direction with different water depth is shown in Figure 6 as characteristic lines $l_{x\text{-}z}$. The sediment concentration is lower in the middle of the main stream region, while it is higher on both sides with a sudden increase in each characteristic line. According to the figure, the dimensionless sediment concentration is C^* = 1.03 - 1.08 in the main stream zone, and C^* = 1.15 - 1.23 on both sides in the forebay. From the forebay's centre to its edges, the concentration of slit increases significantly. As illustrated in Figures 6a and b, the flow diffuses more and the influence of vortexes and high concentration zones increase from the typical lines $l_{x1\text{-}z1}$ to $l_{x6\text{-}z1}$. It is easy to see where silt has accumulated on the side walls. It demonstrates that increased flow velocity can contribute to sediment-carrying capacity, resulting in lower sediment concentration and accumulation. The forebay's *Z*1 section with α = 25° has a maximum sediment concentration of C^* = 1.205, which is 1.4 % lower than the prototype pumping station forebay.

Figures 6c and d illustrate the distribution of sediment concentration along a specific characteristic line in the forebay with different diffusion angles. The concentration is lowest in the centre and highest on either side. The maximum sediment concentration and concentration zone both decrease as the diffusion angle decreases. Because of the sidewall limitation, flow velocity increases, resulting in a reduction in vortex scale and sediment concentration. It may be determined that reducing the forebay diffusion angle can effectively improve sediment deposition.

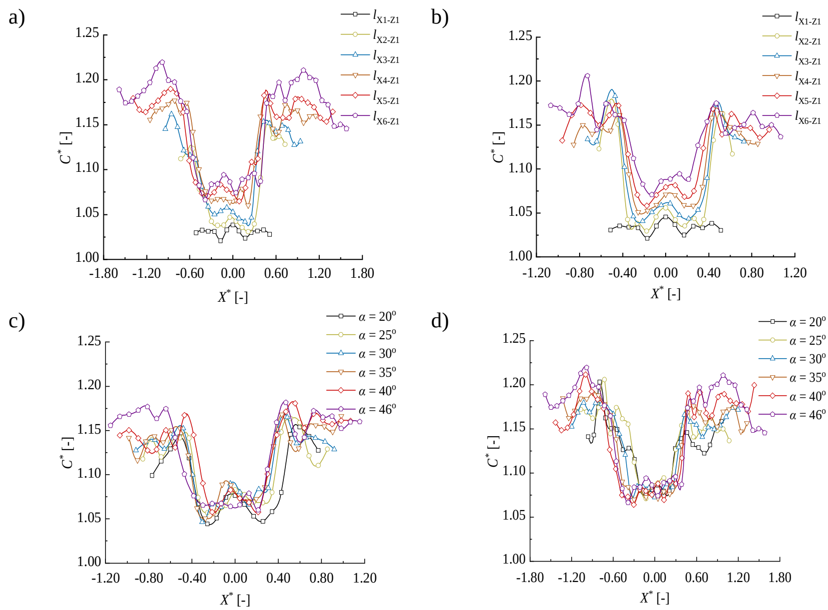

Fig. 6. The sediment concentration distribution on different observation characteristic lines of a) $\alpha = 46°$, b) $\alpha = 25°$; and the flow velocity distribution on c) line $l_{X4\text{-}Z1}$, d) line $l_{X6\text{-}Z1}$ in the forebay with different diffusion angles

Sediment distribution along the water depth

Figure 7 depicts the surface area of high concentration distribution along the water depth in the pumping station forebay with different α. The high concentration zones gradually decrease from the pool's bottom to water's surface. The area of high sediment is 0.71 at the *Z*1 plane and drops dramatically to roughly 0.1 m after 1.2 m rise to the Z7 plane in the forebay with $\alpha = 46°$. Actually, as the water depth increases, flow velocity decreases. Furthermore, the stagnation in the core of the vortex reduces the flow's sediment-carrying capacity. Thus the sediment concentration may surpass the flow's sediment-carrying capacity, resulting in sediment buildup.

The high concentration zones become significantly smaller as the diffusion angle decreases. The surface area of high sediment at the *Z*1 plane is 0.37 in the forebay with $\alpha = 20°$, decreases by almost 57 % compared to the prototype forebay at the same plane. When the diffusion angle lowers, so does the sediment volume, the volume is 82% of the starting sediment in the forebay with $\alpha = 35°$, compared to about 43 % at $\alpha = 20°$. Thus, lowering the diffusion angle can reduce sediment accumulation and increase discharge capacity.

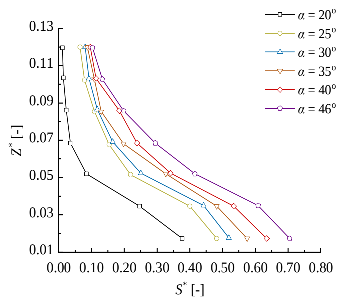

Fig. 7. The surface area of high sediment concentration distribution in forebays with different α

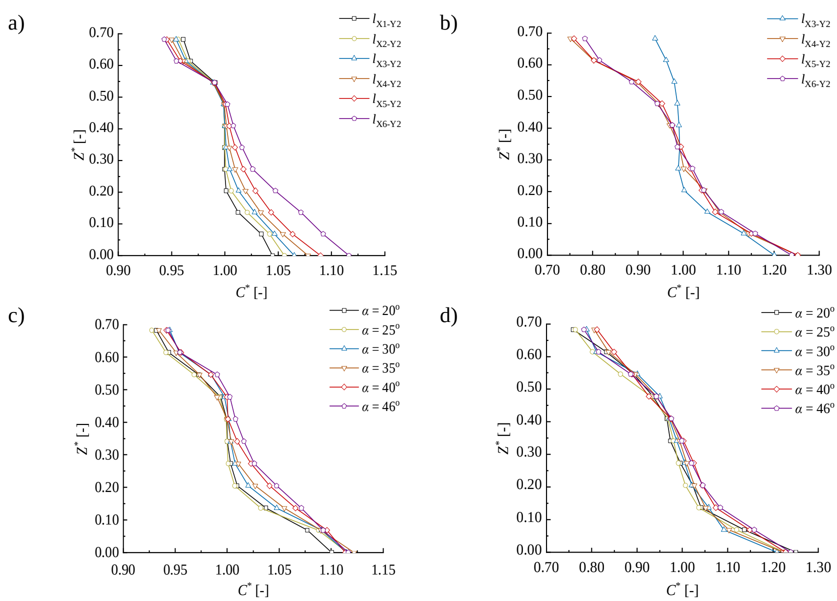

Fig. 8. Sediment concentration distribution on different observation characteristic lines at the forebay of a) α = 46°, b) α = 25°; and flow velocity distribution on c) line $l_{X6\text{-}Y2}$, d) line $l_{X6\text{-}Y3}$ in the forebay with different diffusion angles

Figure 8 shows the distribution of sediment concentrations along the characteristic lines $l_{x\text{-}y}$ in the forebay with various water depths. The sediment concentration gradually declines from the pool bottom to the water's surface. For example, along the line $l_{x6\text{-}y2}$ in the forebay with α = 46°, the dimensionless sediment concentration is C^* = 1.11 near the pool bottom, but drops 15 % at the top, as shown in Figure 8a. The silt in the main flow section and along the sidewalls are contrasted here. Even the averaged sediments are closed during the major flow and backflow sections, while their ranges vary. The dimensionless sediment concentration at the both sidewalls ranges from 1.25 at the base to 0.75 near the water's surface (as illustrated in Fig. 8b). It depicts that the vortexes in backflow zones are stronger, and the flow sediment-transport capacity is weaker when close to the pool base. As shown in Figure 8c, sediment concentrations in the forebay under different diffusion angles are similar and increase with water depth. The sediment distributions on line $l_{X6\text{-}Y3}$ with different diffusion angles are bigger in extent than the distributions on line $l_{X6\text{-}Y2}$ (shown in Figs. 8c and d), indicating that the vortex has a significant impact on sediment accumulation.

The deposition efficiency and flow velocity

The effectiveness of the sediment deposition in the forebay was determined using equation:

$$\eta = \frac{C_{in} - C_{out}}{C_{in}} \tag{5}$$

where C_{in} and C_{out} represent the average volume of sediment concentration at the entrance and exit of the forebay, respectively. Figure 9 depicts the link between sediment deposition efficiency and the forebay with different diffusion angles. The efficiency increases with the diffusion angle α. The deposition rate is 0.74 % when α = 20°, but it climbs to around 3.35 % when α = 46°. Moreover, sediment concentration is strongly proportional to flow velocity. The sediment concentration decreases with flow velocity, as shown in Figure 10. The fitting curve is $v = 0.0028C^2 - 0.0065C + 0.015$, and the correlation coefficient is $R^2 = 0.96$. These results demonstrate that changing the diffusion angle can boost flow velocity while lower sediment deposition rate and accumulation in the forebay.

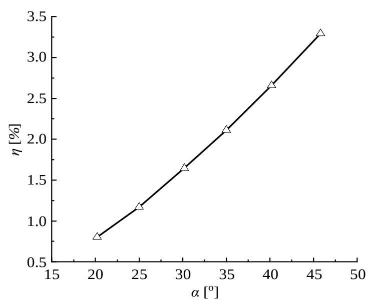

Fig. 9. The changing of the sediment deposition efficiency in the forebay with diffusion angle α

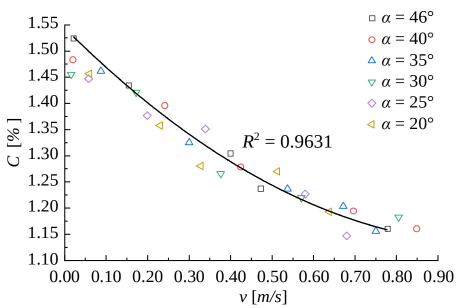

Fig. 10. The relationship between sediment concentration and flow velocity

Conclusion

This study employs numerical modelling and field investigation to examine the properties of sediment concentration distribution in a large-scale front inflow forebay with different diffusion angles. The key findings are as follows:

- First, the flow field has a symmetrical distribution, with the main flow zone in the centre and the backflow sections on both sides with vortices in the forward inflow forebay. When the diffusion angle of the front pool falls, the sidewalls will hinder the flow less. Hence, reducing the diffusion angle of the front inlet forebay can improve the flow patterns and boost the flow stability except at extremely small angles.
- Second, the high sediment concentration is in the centre of the forepond, and the low sections are near both sidewalls. The massive sediment accumulation may be seen in the backflow regions of the forebay with a high diffuse angle. As the diffusion angle decreases, the high concentration area drops, while the low concentration area grows. Thus, a small-angle forebay can increase the flow's sediment-carrying capacity and effectively improve sediment buildup.
- Third, the sediment concentration is lower in the centre of the main stream region, but it is high on both sides, with a dramatic increase in each characteristic lines of $l_{x\text{-}z}$. The sediment concentration increases significantly from the centre of the forebay to both flanks. It demonstrates that the high flow velocity could contribute to the sediment-carrying capacity, and then to lower sediment concentration and accumulation. It is found that when the diffusion angle is 25° - 30°, the differences in flow layer flow field structures are minimal, and both the water flow diffusion effect and flow field structure are optimal.

Moreover, as the water depth in the forebay with different α, the high sediment concentration zones gradually decrease from the pool's bottom to the surface. With the water depth increases, the flow velocity lower down and the sediment concentration exceeds the flow's sediment-carrying limit, causing sediment buildup. What's more, when the diffusion angle decreases, the high concentration zones become significantly smaller. And the sediment volume decreases with the drop of the diffusion angle. Backflow zones have stronger vortexes and flow sediment-transport capacity is lower when near to the water depth. Sediment concentrations are consistent in the forebay with different diffusion angles and increase with water depth. The vortex has a significant impact on sediment accumulation.

Finally, the efficiency of the sediment deposition increases with the diffusion angle α. The sediment concentration decreases with flow velocity, and the fitting curve is $v = 0.0028C^2 – 0.0065C + 0.015$ with a correlating coefficient of $R^2 = 0.96$. It is possible to decrease the rate of sediment deposition, raise flow velocity, and prevent sediment buildup in the forebay by decreasing the diffusion angle. In fact, the Jingtaichuan Pumping Irrigation Project in China is using this work to reconstruct its forebay. It greatly increases the capacity for watering in the irrigation area and improves sediment accumulation.

Acknowledgments

The National Natural Science Foundation (42167043), the Natural Science Foundation of Gansu Province (21JR7RA238), the Water Conservancy Science Experiment Research and Technology Promotion Project of Gansu Province (20GSLK070, 23GSLK038, 24GSLK023) are acknowledged by the authors for their financial support.

References

[1] Zhao JX. An empirical study on emissions trading influence for the enterprise environmental responsibility. Ecol Chem Eng S. 2023;30(2):259-66. DOI: 10.2478/eces-2023-0027.

[2] Li R. Evaluating the development path of manufacturing industry under carbon neutralisation. Ecol Chem Eng S. 2023;30(4):581-93. DOI:10.2478/eces-2023-0042.

[3] Luo C, He Y, Shang Y, Cong X, Ding C, Cheng L, et al. Flow characteristics and anti-vortex in a pump station with laterally asymmetric inflow. Processes. 2022;10:2398. DOI: 10.3390/pr10112398.

[4] Sabouki MM, Bahrainian SS, Behbahani-Nejad M. Numerical investigation of vortex formation in water intake system of a pumping station during low and high tides. SN Appl Sci. 2021;3:1-14. DOI: 10.1007/s42452-020-04048-4.

[5] Zi D, Shen L, Xuan AQ, Wang JF. LES analyses of the air-core vortex in intake flow field of pumping station. IOP Conf Ser: Earth Environ Sci. IOP Publishing. 2019;240:032037. DOI: 10.1088/1755-1315/240/3/032037.

[6] Xu C, Tian J, Liu Z, Wang R, Wang G. Three-dimensional reverse modeling and hydraulic analysis of the intake structure of pumping stations on sediment-laden rivers. Water Resources Manage. 2023;37:537-55. DOI: 10.1007/s11269-022-03385-w.

[7] Urishev B, Artikbekova F, Kuvvatov D, Nosirov F, Kuvatov U. Trajectory of sediment deposition at the bottom of water intake structures of pumping stations. IOP Conf Series: Materials Sci Eng. IOP Publishing. 2021;1030:012137. DOI: 10.1088/1757-899x/1030/1/012137.

[8] Khudair BH. Influent flow rate effect on sewage pump station performance based on organic and sediment loading. J Eng. 2019;25:1-11. DOI: 10.31026/j.eng.2019.09.1.

[9] Zhou J, Zhao M, Wang C, Gao Z. Optimal design of diversion piers of lateral intake pumping station based on orthogonal test. Shock Vibration. 2021;2021:6616456. DOI: 10.1155/2021/6616456.

[10] Zi D, Wang FJ, Yao ZF, Xiao RF, Chen X, He CL. Numerical simulation on rectifying flow in intake system of a pumping station connected with headrace pipe. IOP Conf Series: Earth Environ Sci. IOP Publishing. 2016;49:032004. DOI: 10.1088/1755-1315/49/3/032004.

[11] Luo C, Cheng L, Liu C, Zhou JR, Jin Y. Numerical simulation of flow pattern with sill in the front inflow forebay of pumping station. IOP Conf Series: Earth Environ Sci. IOP Publishing. 2012;15:052006. DOI: 10.1088/1755-1315/15/5/052006.

[12] Shi W, Lv F, Yu X, Wang X, Ni C, Lu W, et al. Influence of partition wall length on inlet flow regime of a pumping station arranged in parallel with a sluice gate. Processes. 2024;12:699. DOI: 10.3390/pr12040699.

[13] Xu B, Xu S, Xia H, Liu J, Shen Y, Xu L, et al. Optimal design of perforated diversion wall based on comprehensive evaluation indicator and response surface method: A case study. Processes. 2023;11:1539. DOI: 10.3390/pr11051539.

[14] Xu B, Liu J, Lu W, Xu L, Xu R. Design and optimization of γ-shaped settlement training wall based on numerical simulation and CCD-response surface method. Processes. 2022;10:1201. DOI: 10.3390/pr10061201.

[15] Xi W, Lu WG, Wang C, Xu B. Optimization of the hollow rectification sill in the forebay of the pump station based on the PSO-GP collaborative algorithm. Shock Vibration. 2021;2021:6618280. DOI: 10.1155/2021/6618280.

[16] Zhou J, Zhao M, Wang C, Gao Z. Influence of different lateral bending angles on the flow pattern of pumping station lateral inflow. Shock Vibration. 2021;2021:6653001. DOI: 10.1155/2021/6653001.

[17] Teaima IR, El-Gamal T. Improving flow performance of irrigation pump station intake. J Appl Water Eng Res. 2017;5:9-21. DOI: 10.1080/23249676.2015.1105160.

[18] Song W, Pang Y, Shi X, Xu Q. Study on the rectification of forebay in pumping station. Mathematical Problems Engineering. 2018;2018:2876980. DOI: 10.1155/2018/2876980.

[19] Zheng X, Zhang P, Zhang W, Yu Y, Zhao Y. Numerical study on the influence of combined rectification facilities on the flow in the forebay of pumping station. Water. 2023;15:3847. DOI: 10.3390/w15213847.

[20] Nasr A, Yang F, Zhang Y, Wang T, Hassan M. Analysis of the flow pattern and flow rectification measures of the side-intake forebay in a multi-unit pumping station. Water. 2021;13:2025. DOI: 10.3390/w13152025.

[21] Li Y, Feng J, Zhu G, Zhou Y, Zhang Y. Evolution of air-entraining vortices in inclined intake pumping stations under low sump water depth condition. Proc Institution Mechanical Engineers. Part E: J Process Mechanical Eng. 2023;09544089231215898. DOI: 10.1177/09544089231215898.

[22] Zheng X, Wang W, Zhang P, Pu Y, Zhao Y. Internal flow characteristics of centrifugal pumps under different startup combination schemes. Water. 2024;16:1087. DOI: 10.3390/w16081087.

[23] Tang Q, Xie W, Jing S, Wang X, Su Z. Experimental and numerical investigation on the mechanical behavior of rock-like material with complex discrete joints. Rock Mechanics Rock Eng. 2024;1-19. DOI: 10.1007/s00603-024-03784-y.
[24] Xu C, Tian J, Wang G, Lian H, Wang R, Hu X. Numerical analysis of water-sediment flow fields within the intake structure of pumping station under different hydraulic conditions. Water. 2024;16:779. DOI: 10.3390/w16050779.
[25] Kartushinsky A, Tisler S, Oliveira JG, Van der Geld CWM. Eulerian-Eulerian modelling of particle-laden two-phase flow. Powder Technol. 2016;301:999-1007. DOI: 10.1016/j.powtec.2016.07.053.
[26] Li L, Xu Y, Ge M, Wang Z, Li S, Zhang J. Numerical investigation of cavitating jet flow field with different turbulence models. Mathematics. 2023;11:3977. DOI: 10.3390/math11183977.
[27] Takizawa K, Bazilevs Y, Tezduyar TE. Isogeometric discretization methods in computational fluid mechanics. Mathematical Models Methods Appl Sci. 2022;32:2359-70. DOI: 10.1142/s0218202522020018.
[28] Liu YY, Yang LM, Shu C, Zhang HW. Three-dimensional high-order least square-based finite difference-finite volume method on unstructured grids. Physics Fluids. 2020;32. DOI: 10.1063/5.0032089.